Available online at www.sciencedirect.com
SCIENCE DIRECT
Journal of Catalysis 242 (2006) 142–152
JOURNAL OF CATALYSIS
www.elsevier.com/locate/jcat

Reaction kinetic analysis of the gas-phase epoxidation of propylene over Au/TS-1

Bradley Taylor [a], Jochen Lauterbach [b], Gary E. Blau [a], W. Nicholas Delgass [a,*]

[a] *Forney Hall of Chemical Engineering, Purdue University, 480 Stadium Mall Drive, West Lafayette, IN 47907-2100, USA*
[b] *Department of Chemical Engineering, University of Delaware, Newark, DE 19716, USA*

Received 10 April 2006; revised 1 June 2006; accepted 3 June 2006

Available online 7 July 2006

Abstract

The superior activity and stability of Au/TS-1 catalysts has allowed the first comprehensive kinetic analysis of the propylene epoxidation system in the absence of significant deactivation. A unique design of experiments combining the best features of factorial experiments with one-at-a-time experimentation over the nonflammable range was used to collect kinetic information, from which a power rate law was extracted using the statistical software package JMP. Explaining the resultant fractional reactant orders ($O_2 = 0.31 \pm 0.04$, $H_2 = 0.60 \pm 0.03$, and $C_3H_6 = 0.18 \pm 0.04$) requires a sequence of elementary kinetic steps having a minimum of two active sites participating in the rate-determining step. A reaction sequence is proposed that accounts for the experimentally determined reaction orders and is consistent with DFT calculations and other results from the literature. This mechanism suggests that titanium and gold sites must generate and use the epoxidation oxidant simultaneously rather than sequentially, as previously suggested in the literature.

Keywords: Kinetic analysis; Propylene epoxidation; Gold catalysts; Titanium silicalite-1; TS-1; Design of experiments; Propylene oxide

1. Introduction

With the discovery of propylene epoxidation activity in the Au–Ti system by Haruta et al. [1], considerable effort has been made to understand the nanoscale gold particle size effects [1–4] and the elemental synergy between gold and titanium that result in this unique selective oxidation activity [1,5–8]. Although an enhanced understanding of the chemical and physical properties of these materials has recently led to catalysts with industrially interesting propylene epoxidation rates [9,10], mechanistic information derived from kinetic experiments has been limited, due in part to the poor stability and reproducibility of many catalysts in the Au–Ti system. With the introduction of catalysts consisting of highly dispersed titanium centers and low gold loadings, the on-stream stability has improved considerably, culminating in Au/TS-1 catalysts capable of the stable production of propylene oxide (PO) for periods exceeding 45 h [10]. Nevertheless, reproducibility problems in catalyst synthesis prevent direct comparison of activity based on metal loading or gold particle size. In addition, the need for two reductants and an oxidant for the reaction entails safety considerations. Traditional experimental methods involving the manipulation of one reaction variable at a time make it necessary to operate at process conditions remote from a standard feed of 10/10/10/70 vol% $O_2/H_2/C_3H_6$/diluent, to have a sufficiently large range of compositions outside of the explosion limit conducive to estimating reliable reaction orders. The kinetic parameters provided by Haruta et al. [1], for example, were obtained from kinetic information far from the standard evaluation conditions, which raises the question of whether data collected under these conditions necessarily reflect the kinetics of the more widely studied 10/10/10/70 vol% $O_2/H_2/C_3H_6$/diluent reactant mixture.

This work takes advantage of the high activity and stability of catalysts prepared by deposition precipitation of gold onto titanium silicalite-1 to determine reaction orders, rate constants, and apparent activation energies from a large number of variable levels. It has ultimately allowed the proposal of a viable

* Corresponding author. Fax: +1 765 494 0805.
E-mail address: delgass@ecn.purdue.edu (W.N. Delgass).

0021-9517/$ – see front matter
doi:10.1016/j.jcat.2006.06.007

epoxidation mechanism over these materials. Utilization of a design of kinetic experiments in which all manipulated variables are changed simultaneously permits the examination of a wide range of nonflammable reaction conditions near the standard evaluation conditions. Another attribute of this design is the ability test for the effects of deactivation and/or catalyst reproducibility. Finally, the experimental design is inherently efficient and permits evaluation of the entire experimental region in a balanced fashion with the ability to check for any synergisms or interactions among the reaction conditions and resultant model parameters.

2. Experimental

2.1. Hybridized factorial design of experiments

An experimental design was constructed to meet the following requirements: (1) easily attained feed conditions, (2) measurable changes in expected product rates, and (3) operations maintained outside the flammability region. Based on exploratory experimental observations, the oxygen concentration ranged from 2 to 8 mol%, whereas the hydrogen and propylene concentrations ranged from 8 to 24 mol%. In addition, Au/TS-1 catalysts temperatures ranged from 140 to 200 °C. Higher temperatures were not examined because of irreversible deactivation of the catalyst. Lower temperatures were neglected to avoid confounding the kinetics with the accumulation of PO on the surface. Based on exploratory experiments, the choice was made to use 15 °C increments over this 60 °C temperature range.

The design itself consists of a hybridization of a factorial design and the traditional one-at-a-time approach familiar to catalyst experimenters. As shown schematically in Fig. 1, the first portion of the design consists of incremental changes in temperature under constant reactant compositions, which can be used to give estimates of the activation energy and pre-exponential factor using a logarithmic transformation. The second portion of the design consists of step changes in oxygen compositions, resulting in the ability to extract an effective oxygen order independent of other factors. The final portion of the experimental design consists of a symmetrical partial factorial design for hydrogen and propylene that has been linked to the first two portions through the use of intermediate temperatures and concentrations. The design consisted of 29 distinct reaction conditions, plus 4 replicates to assess experimental error and check for catalyst deactivation. The reaction conditions (5/12/12/71 vol% $O_2/H_2/C_3H_6$/diluent, 170 °C) were chosen as the replicate conditions because they consist of roughly midpoint values of the four process variables. It was felt that repeating this middle point would serve as a good measure of variability over the entire operating region.

2.2. Catalyst preparation and characterization

Two titanium silicalite-1 samples were synthesized in micellar media [11] and named according to the silicon-to-titanium molar ratio such that Si/Ti = 36 is denoted by TS-1(36) and Si/Ti = 143 is denoted by TS-1(143). The specifics of the preparation, as well as the characterization of these support materials, have been presented previously [10]. A typical synthesis gel began with the addition of 3.5 g of polyoxyethylene 20-sorbitan monolaurate (Tween® 20, Fischer Scientific, Enzyme Grade) to 56 mL of deionized water under vigorous stirring. This was followed by dropwise addition of 26 mL of tetrapropylammonium hydroxide (TPAOH, Aldrich, 40 wt%), followed by dropwise addition 66.5 mL of tetraethylorthosilicate (TEOS, Aldrich, >98%). The solution was then stirred for 1 h. A solution consisting of up to 3 mL of titanium (IV) butoxide (TBOT, Aldrich, >98%) in 20 mL of isopropyl alcohol (IPA, Mallinckrodt, ChromAR) was then added dropwise under stirring. The final solution was stirred for a minimum of 1 h before being placed in a Teflon autoclave at 140 °C for 18 h. The resulting solid was separated from the growth liquid via centrifugation, washed thoroughly with approximately 100 mL of room temperature deionized water, and dried overnight at room temperature in a vacuum oven. Once dry, the resulting white

Exp #	T (°C)	Volume % O_2	H_2	C_3H_6
1	170	5	12	12
2	140	5	12	12
3	155	5	12	12
4	185	5	12	12
5	200	5	12	12
6	170	5	12	12
7	170	2	12	12
8	170	3.5	12	12
9	170	6.5	12	12
10	170	8	12	12
11	170	5	12	12
12	170	5	8	12
13	170	5	16	12
14	170	5	12	8
15	170	5	12	16
16	170	5	12	12
17	155	3.5	16	16

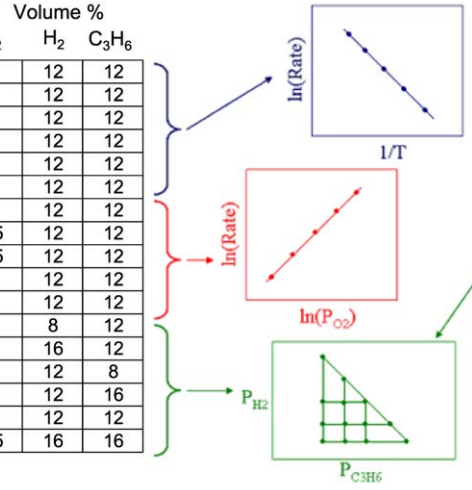

Exp #	T (°C)	Volume % O_2	H_2	C_3H_6
18	155	3.5	24	8
19	155	3.5	8	24
20	155	3.5	8	8
21	185	3.5	20	12
22	185	3.5	12	20
23	185	3.5	8	16
24	185	3.5	16	8
25	155	6.5	8	24
26	155	6.5	16	16
27	155	6.5	8	8
28	155	6.5	24	8
29	185	6.5	20	12
30	185	6.5	12	20
31	185	6.5	16	8
32	185	6.5	8	16
33	170	5	12	12

Fig. 1. A schematic showing a breakdown of the hybridized factorial design of kinetic experiments. The first two portions of the design are similar to traditional kinetic analysis in which only one variable is changed at a time, while the final portion is a true factorial design.

Table 1
Characterization of examined catalysts

Catalyst	Bulk Si/Ti	Ti loading (wt%)	Support particle diameter (nm)	Gold content of DP solution (g/L)	Gold loading (wt%)
0.04Au/TS-1(143)	143	0.56	261 ± 18	2.36	0.04
0.06Au/TS-1(36)	36	2.2	355 ± 59	2.49	0.06
0.02Au/TS-1(36)	36	2.2	355 ± 59	1.13	0.02

powder was calcined at 535 °C for at least 8 h to remove the organic template. A typical preparation utilizing 3 mL of TBOT resulted in 8 g of zeolite with a titanium content of approximately 2 wt%. X-ray diffraction patterns showed the crystal structure to be orthorhombic MFI, whereas diffuse reflectance ultra-violet/visible (DRUV–vis) spectra were consistent with the ligand-to-metal charge transfer for tetrahedral titanium inserted into the zeolite framework.

Gold was deposited using the method of deposition precipitation (DP) as outlined by Tsubota et al. [12]. An appropriate amount of hydrogen tetrachloroaurate(III) ($HAuCl_4 \cdot x H_2O$, Alfa Aesar, 99.999%) was dissolved in 50 mL of deionized water, resulting in the gold solution concentrations given in Table 1. Following suspension of approximately 1 g of calcined support material in the gold precursor solution, the slurry was neutralized to a pH of 9 using a saturated aqueous solution of sodium carbonate. The slurry was stirred for 4 h at room temperature, after which the solid was removed via centrifugation, resuspended in approximately 50 mL of deionized water, separated again by centrifugation, and dried under vacuum at room temperature. In general, <2% of the available gold in solution was deposited on the support material. Gold loading was determined by atomic absorption spectroscopy (AAS) using a Perkin Elmer AAnalyst 300, and support particle size distributions were determined using a JEOL 2000FX transmission electron microscope (at 200 keV) outfitted with a charge coupled device camera. TEM images are omitted here because of a lack of discernible gold particles; representative TEM images of the support materials can be found elsewhere [10]. Catalysts were named for gold loading and the support material, as shown in Table 1.

2.3. Kinetic evaluation

Kinetic measurements were made using a 1/2-inch-diameter steel vertical reactor operating at differential conversion. Catalysts were sieved to 60–80 mesh. The reaction rates were measured in a reactant mixture of oxygen (99.999%), hydrogen (99.999%), propylene (99.9%), and nitrogen (99.999%) with a total flow rate of approximately 55 sccm and a resulting space velocity of 7000 mL/(h g_{cat}). The measured rates are shown in Fig. 2. The effects of deactivation were minimized by conducting the kinetic experiments within 24 h of the preparation of each catalyst. Each catalyst was evaluated without any pretreatment and activated on stream in a 10/10/10/70 vol% mixture of $O_2/H_2/C_3H_6/N_2$ at 200 °C. For catalyst 0.04Au/TS-1(143), the reactor effluent was separated using a Varian 3700 gas

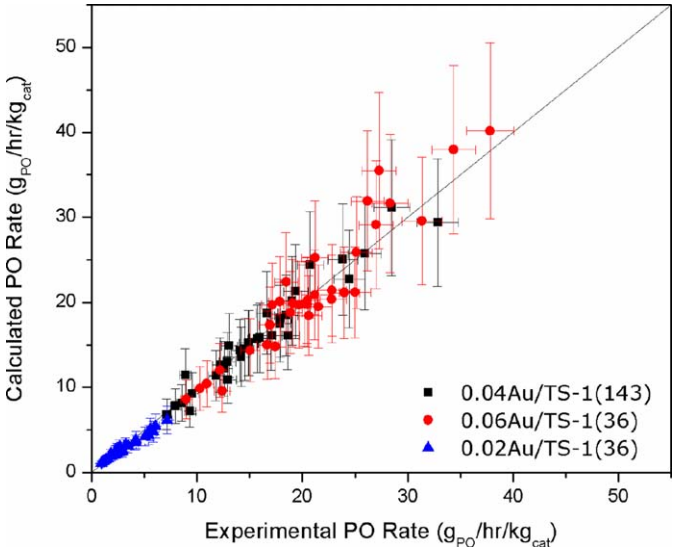

Fig. 2. Parity plot for the power rate law fit to kinetic data including 95% confidence intervals obtained from fitting catalysts 0.04Au/TS-1(143), 0.06Au/TS-1(36) and 0.02Au/TS-1(36).

chromatograph. Organic products were separated using a Supelcowax 10 capillary column (0.53 mm × 60 m) and analyzed using a flame ionization detector. Inorganic products were separated using a Chromosorp 102 packed column (1/8 inch × 8 ft) and analyzed using a thermal conductivity detector. Effluents from catalysts 0.06Au/TS-1(36) and 0.02Au/TS-1(36) were analyzed identically to those of 0.04Au/TS-1(143), except that an Agilent 6890N GC was used. Each catalyst was maintained at the conditions outlined in the experimental design for at least 30 min before analysis of the reactor effluent. A minimum of three samples was collected at each experimental condition to assess the variability in the sampling and analytical measurement. Hydrogen efficiency was calculated directly. However, use of a nitrogen carrier gas prevented the quantification of carbon dioxide and the reporting of accurate product selectivities. Although carbon dioxide was previously found to be the most abundant side product in this laboratory, selectivity to carbon dioxide was still below 10% [10]. External mass transfer limitations were eliminated by operating at a high space velocity. Internal mass transfer limitations were neglected because the Thiele modulus was estimated to be <1.

2.4. Data analysis

A log transformation of the rate data generated by the design of experiments was fit to a power rate law using the linear regression features of the statistical software package JMP, version 5.0.1a. To decrease parametric interaction between the preexponential factor and the apparent activation energy, all data points were referenced to the rate constant obtained at 170 °C. Because there is no way to count the number of active sites on each catalyst, any fits involving more than one catalyst include a bias that serves as a fitting parameter and accounts for the relative difference in the number of active sites. Care was taken to ensure proper weighting of the data. To fully account for the differing number of data points per experimental condition, the

Table 2
Power rate law parameters obtained for catalysts 0.04Au/TS-1(143), 0.06Au/TS-1(36) and 0.02Au/TS-1(36). Rate expression ($g_{PO}/(h\,kg_{cat})$)

$$\text{PO rate} = k_{170\,^\circ C}(\text{Bias})e^{-\frac{E_a}{R}\left[\frac{1}{T}-\frac{1}{443K}\right]}[O_2]^x[H_2]^y[C_3H_6]^z$$

Parameter	Value	95% conf. int.
$k_{170\,^\circ C}$ ($g_{PO}/(h\,kg_{cat}\,atm^{x+y+z})$)	256	56
E_a/R (K)	5077	166
x	0.31	0.04
y	0.60	0.03
z	0.18	0.04
0.04Au/TS-1(143) bias	1	–
0.06Au/TS-1(36) bias	1.33	0.03
0.02Au/TS-1(36) bias	0.15	0.01
R^2	0.9878	

standard deviation and statistical error for each reaction condition were propagated through the model.

3. Results

A total of 33 kinetic measurements were performed over the course of more than 100 h on stream for each of three catalysts. The experiments were run in the order presented in Fig. 1, with the exception of (185 °C, 6.5/12/20/61.5 vol% $O_2/H_2/C_3H_6/N_2$) for catalyst 0.04Au/TS-1(143), which was completed following (185 °C, 6.5/8/16/69.5 vol% $O_2/H_2/C_3H_6/N_2$). The actual compositions and rate data are given in Tables A1–A3 in Appendix A. Slight deactivation (<6%) of catalyst 0.04Au/TS-1(143) occurred during one of the kinetic experiments (185 °C, 6.5/12/20/61.5 vol% $O_2/H_2/C_3H_6/N_2$). This had little effect on the subsequent kinetic experiments, because the change fell within the statistical error of the rate measurement (∼6%), and the only remaining kinetic experiment was the re-evaluation of (170 °C, 5/12/12/71 vol% $O_2/H_2/C_3H_6/N_2$). There was no evidence of deactivation for catalysts 0.06Au/TS-1(36) or 0.02Au/TS-1(36), perhaps due to the shorter time required to obtain the data and analyze the results using the Agilent 6890N gas chromatograph. The partial pressures of hydrogen, oxygen, propylene, and PO were measured directly using gas chromatography, whereas the partial pressure of water was estimated from the conversion of hydrogen across the catalyst bed. Hydrogen selectivity (efficiency) was defined as the number of moles used to produce PO (because $H_2 + O_2 + C_3H_6 \rightarrow PO + H_2O$) divided by the total number of moles of hydrogen consumed. The average partial pressures of oxygen, hydrogen, propylene, PO, and water, along with the PO production rate for each of the 33 experiments and 3 catalysts, were supplied to JMP 5.0.1a, and the power rate law, depicted in Table 2, was fit by varying the pre-exponential factor referenced to 170 °C, activation energy, reactant orders, product orders, and a bias parameter to account for differences in the number of active sites between catalysts. Both PO and water were found to have little effect on the model fit and were ultimately neglected in the reporting of the final parameters, shown in Table 2. The model parity plot is shown in Fig. 2, and a plot of model residuals is given in Fig. 3. The overall model fit is good, with an adjusted R^2 value of 0.9878. The PO

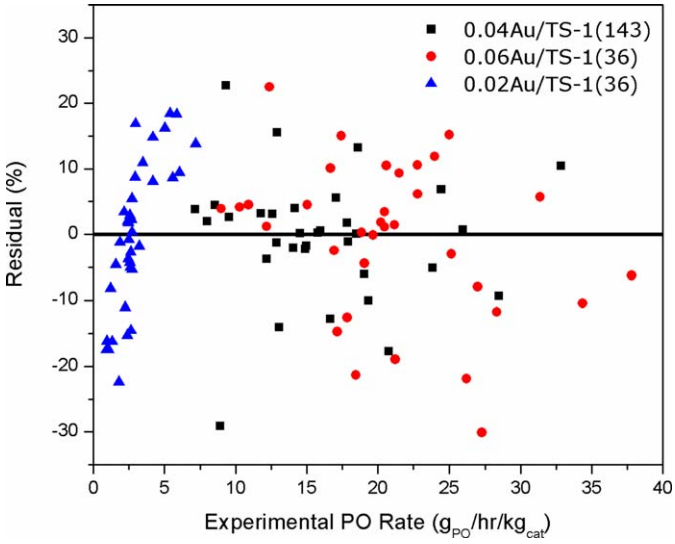

Fig. 3. Percent residual in the power rate law fit for catalysts 0.04Au/TS-1(143), 0.06Au/TS-1(36) and 0.02Au/TS-1(36).

Table 3
Power rate law parameters for a fit only to catalyst 0.02Au/TS-1(36). Rate expression ($g_{PO}/(h\,kg_{cat})$)

$$\text{PO rate} = k_{170\,^\circ C}(\text{Bias})e^{-\frac{E_a}{R}\left[\frac{1}{T}-\frac{1}{443K}\right]}[O_2]^x[H_2]^y[C_3H_6]^z$$

Parameter	Value	95% conf. int.
$k_{170\,^\circ C}$ ($g_{PO}/(h\,kg_{cat}\,atm^{x+y+z})$)	36	7
E_a/R (K)	6609	151
x	0.30	0.05
y	0.60	0.03
z	0.16	0.04
R^2	0.9850	

rate was found to be most dependent on hydrogen partial pressure, whereas propylene partial pressure had the least effect. As shown in Fig. 2, all of the points fell within the 95% confidence interval of the parity line. When recast as rate, rather than the natural log of rate, the error in the four parameters, all of which are exponents [the software fits $\ln(k)$ rather than k to retain a linear model], increased sharply, as expected. As stated previously, the bias parameters are meant to account for differences in the number of active sites among a group of catalysts; therefore, a 0.06Au/TS-1(36) bias of 1.33 ± 0.03 has a physical interpretation that catalyst 0.06Au/TS-1(36) has 33% more active sites than catalyst 0.04Au/TS-1(143), and a 0.02Au/TS-1(36) bias of 0.15 ± 0.01 means that catalyst 0.02Au/TS-1(36) has only 15% of the active sites of catalyst 0.04Au/TS-1(143).

A plot of the residuals on a percentage basis shows that although the overall fit of the power rate law was good, a feature in catalyst 0.02Au/TS-1(36) was not captured by the fit to all three catalysts. Comparing the individual fit of catalyst 0.02Au/TS-1(36) (Table 3) with a combined fit of catalysts 0.04Au/TS-1(143) and 0.06Au/TS-1(36) (Table 4) showed that the discrepancy in Fig. 3 was due to a difference in the apparent activation energies of the catalysts. Plots of these additional fits are given in Figs. 4 and 5, where all of the data points overlap the parity line (i.e., predicted rate equals observed rate). Plots of

Table 4
Power rate law parameters for a fit to catalysts 0.04Au/TS-1(143) and 0.06Au/TS-1(36). Rate expression ($g_{PO}/(h\,kg_{cat})$)

$$\text{PO rate} = k_{170\,^\circ C}(\text{Bias})e^{-\frac{E_a}{R}\left[\frac{1}{T}-\frac{1}{443K}\right]}[O_2]^x[H_2]^y[C_3H_6]^z$$

Parameter	Value	95% conf. int.
$k_{170\,^\circ C}$ ($g_{PO}/(h\,kg_{cat}\,atm^{x+y+z})$)	228	54
E_a/R (K)	4245	173
x	0.28	0.04
y	0.59	0.04
z	0.18	0.04
0.04Au/TS-1(143) bias	1	–
0.06Au/TS-1(36) bias	1.33	0.03
R^2	0.9372	

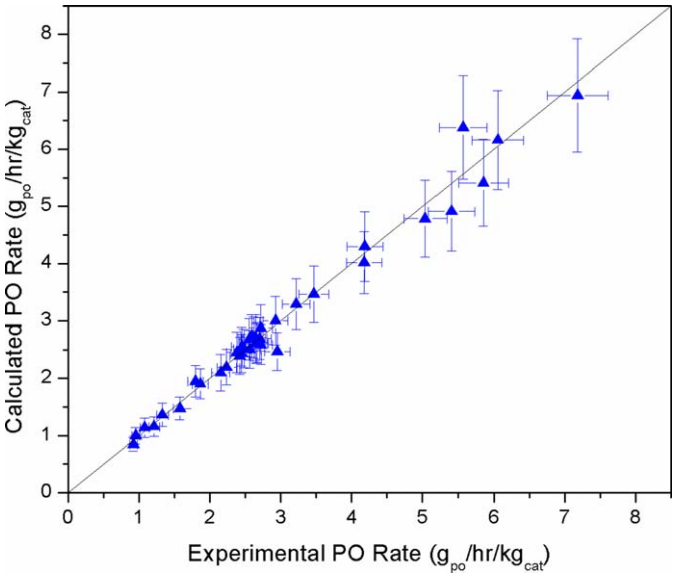

Fig. 4. Parity plot for the power rate law fit to kinetic data including 95% confidence intervals obtained from fitting catalyst 0.02Au/TS-1(36).

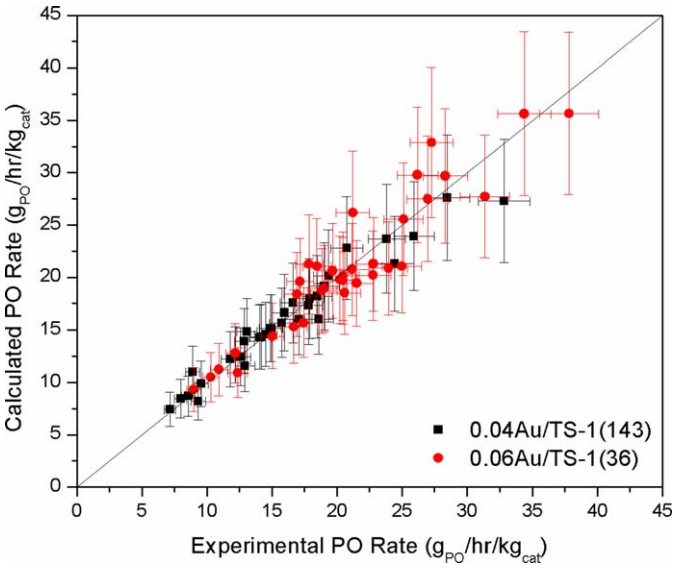

Fig. 5. Parity plot for the power rate law fit to kinetic data including 95% confidence intervals obtained from fitting catalysts 0.04Au/TS-1(143) and 0.06Au/TS-1(36).

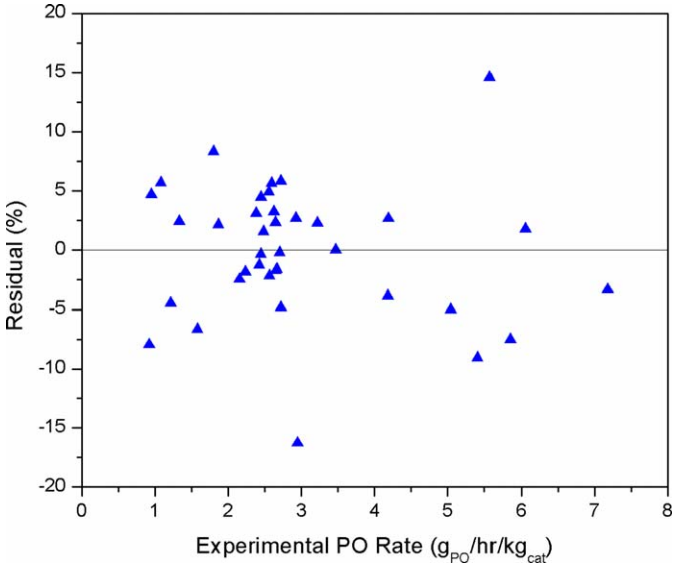

Fig. 6. Percent residual in the power rate law fit for catalyst 0.02Au/TS-1(36).

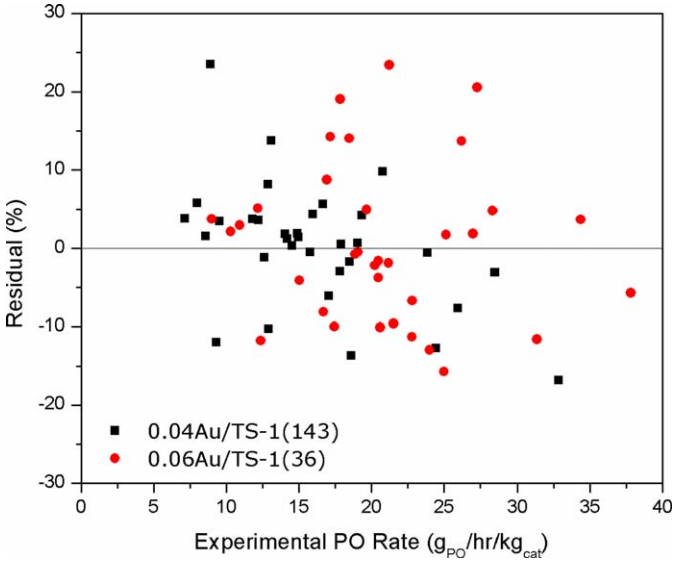

Fig. 7. Percent residual in the power rate law fit for catalysts 0.04Au/TS-1(143), and 0.06Au/TS-1(36).

the residuals in Figs. 6 and 7 show a random distribution about the zero line. The absence of a trend with increasing PO rate (corresponding to an increase in PO and water partial pressure) validates the omission of PO and H_2O in the power rate law, because all of the trends in the data have been efficiently captured using only the reactant orders, as given in Table 2.

As shown representatively using data from catalysts 0.04Au/TS-1(143) in Fig. 8, the hydrogen efficiency and hydrogen consumption rate were measured directly and track the PO production rate. The hydrogen consumption rate and hydrogen efficiency (selectivity) were strongly affected by changes in the reaction mixture. During catalyst activation (the period between 5 and 16 h on stream), the hydrogen selectivity reached a local maximum before decreasing with time on stream. The decrease in hydrogen selectivity is commensurate with an increased consumption of hydrogen despite a constant production of PO. As

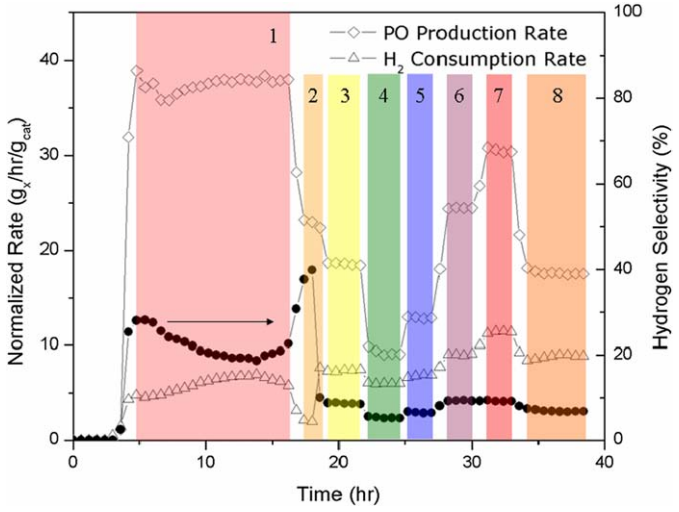

Fig. 8. Normalized PO production rate, H_2 consumption rate and hydrogen selectivity versus time for catalyst 0.04Au/TS-1(143). The shaded regions from left to right represent (1) 200 °C, 10/10/10/70 vol% $O_2/H_2/C_3H_6/N_2$; (2) 170 °C, 10/10/10/70 vol% $O_2/H_2/C_3H_6/N_2$; (3) 170 °C, 5/12/12/71 vol% $O_2/H_2/C_3H_6/N_2$; (4) 140 °C, 5/12/12/71 vol% $O_2/H_2/C_3H_6/N_2$; (5) 155 °C, 5/12/12/71 vol% $O_2/H_2/C_3H_6/N_2$; (6) 185 °C, 5/12/12/71 vol% $O_2/H_2/C_3H_6/N_2$; (7) 200 °C, 5/12/12/71 vol% $O_2/H_2/C_3H_6/N_2$; (8) 170 °C, 5/12/12/71 vol% $O_2/H_2/C_3H_6/N_2$.

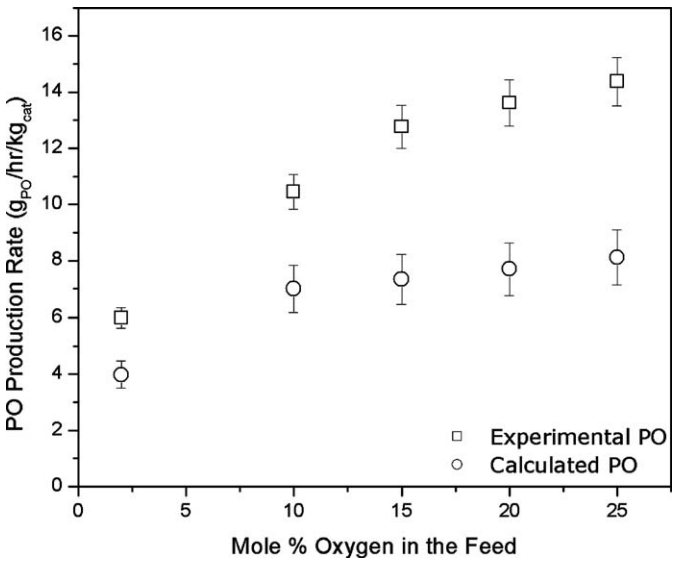

Fig. 9. Experimental and calculated PO rate for catalyst 0.02Au/TS-1(36) using a feed mixture of 2–25 mol% oxygen, 40 mol% hydrogen, 5 mol% propylene and nitrogen as a diluent at 170 °C.

the temperature was lowered to 170 °C in preparation for the kinetic experiments, hydrogen consumption dropped sharply. On initiation of region 3 of the experimental protocol, after 19 h on stream in Fig. 8, the hydrogen consumption increased (hydrogen selectivity decreased) sharply despite a decrease in the PO production rate. After this point in the experimental sequence, PO production rate, H_2 consumption rate, and H_2 selectivity all tracked with one another, with the exception of the region at 28–33 h on stream (regions 6 and 7), in which the hydrogen efficiency remained unchanged despite a 15 °C increase in reaction temperature. At 34 h on stream (region 8), the reaction conditions returned to those of the first kinetic experiment (region 3). Despite changes of temperature and an additional 15 h on stream, hydrogen efficiency, hydrogen consumption, and PO production were nearly identical to those at the starting conditions.

Under the conditions examined in the design of experiments, there appeared to be no saturation of the rate with any of the reactant partial pressures. Given that rate saturation with oxygen partial pressure has been observed previously [1], a series of experiments was run on catalyst 0.02Au/TS-1(36) in an attempt to see whether the rate did indeed saturate over Au/TS-1 catalysts. For this series of experiments, hydrogen and propylene were maintained at 40 and 5 mol%, respectively, which allowed variation of the oxygen content from 2 to 25 mol% while limiting the combustibility of the feed. The results, presented in Fig. 9, show that the PO rate did indeed saturate at oxygen partial pressures above 20 mol%. These experiments took place at hydrogen partial pressures much higher and propylene partial pressures much lower than were examined in the hybridized factorial design of experiments. Some of the oxygen partial pressures also exceeded those used in the model fitting. Included in Fig. 9 is a prediction of the PO rate under these conditions to show how well the power rate law represents trends outside of the range of conditions examined in the design of experiments. The power rate law predicted the general shape of the PO rate as a function of oxygen partial pressure, but the absolute PO rate appeared to be shifted by approximately 30%. Because the model is a simple power rate law, it is not capable of reproducing the saturation in rate at higher oxygen partial pressures.

4. Discussion

Traditionally, PO is considered to have very strong adsorption to the catalyst surface and almost certainly to have a negative reaction order due to site blocking [6]. Thus, PO would be expected to appear in the power rate law. Similarly, water content has been found to have a significant effect on the combustion of CO over gold-based catalysts [13] as well as to affect PO rate [14]. The weak interaction between the products and the PO rate is likely due to the higher reaction temperatures used in these experiments relative to other published studies. Most of our data were obtained at 155 °C or higher, as opposed to some of the more prominent studies that focused on reaction conditions below 160 °C [1,5,9]. In addition, the effects of products on the PO rate may also have been diminished by the relatively low activity of the examined catalyst and the use of a space velocity essentially 50% larger than is generally used in the literature (6000–7000 mL/(h g_{cat}) vs. 4000 mL/(h g_{cat})) that culminated in low propylene conversion. Compared with a catalyst prepared from these supports and reported previously [10], these catalysts are only one-third as active at 200 °C in a 10/10/10/70 vol% $O_2/H_2/C_3H_6$/diluent reaction mixture. This relatively low activity corresponds to very small changes in PO partial pressure in the catalyst bed, particularly when these values are placed on a log scale. The reason for this decreased activity is not explicitly known, although cat-

alysts 0.04Au/TS-1(143) and 0.06Au/TS-1(36) were made with a higher concentration of gold precursor in the gold deposition solution. As discussed previously [10], high concentrations of gold in the deposition solution can be detrimental to catalyst activity by forcing the catalyst support to uptake more gold than would be required to produce a stable, active catalyst. However, all of these catalysts were stable under reaction conditions, and thus excess gold loading does not appear to account for the unusually low activity of catalyst 0.02Au/TS-1(36).

An individual fit of catalyst 0.02Au/TS-1(36) showed that the apparent activation energy was significantly greater than that of the other two catalysts while resulting in nearly identical reaction orders. Residual plots of catalysts 0.02Au/TS-1(36) alone and catalysts 0.04Au/TS-1(143) and 0.06Au/TS-1(36) fitted in concert showed no trend in the residual errors with PO rate; therefore, the current set of parameters were sufficient to reproduce the experimental data. We conclude from this analysis that some variation in both pre-exponential factor and activation energy was associated with the specific catalyst preparation, but that there was little effect on the orders of reaction.

The orders of reaction obtained in this study varied significantly from those reported by Haruta et al. [1]. Although the weak dependence on propylene was consistent in both studies, Haruta et al. found the oxygen order to be near 1 and the rate to saturate at concentrations >10 mol%. Haruta et al. also found that the hydrogen orders ranged from 0.6 to 0.9 depending on temperature, which, to a certain extent, is consistent with the value obtained from the factorial experiments. The primary difference between this work and that of Haruta et al. is that although both were active for the epoxidation of propylene, the catalysts are very different chemically. Haruta et al. examined Au/TiO_2 catalysts at much higher gold loadings, at lower temperatures, and in the presence of significant deactivation. Despite the lower activity of the catalysts reported here in comparison to others reported more recently in the literature [9,10], PO was stably produced at three times the rate per gram of catalyst as that presented by Haruta et al. [1].

Careful examination of the hydrogen efficiency during the first 40 h on stream reveals some very interesting relationships between the reaction environment and hydrogen selectivity. Hydrogen selectivity appears to benefit from activation in the 10/10/10/70 vol% $O_2/H_2/C_3H_6/N_2$ with an inexplicable spike in hydrogen selectivity as the temperature is decreased from 200 to 170 °C. Altering the reaction mixture to 5/12/12/71 vol% $O_2/H_2/C_3H_6/N_2$ increased the hydrogen consumption and decreased the hydrogen selectivity with a mere 2% increase in hydrogen concentration. The implication, as has been shown previously by Barton et al. [15], is that the hydrogen order for water production is far greater than that of oxygen. Interestingly, as the temperature was changed from 170 °C down to 140 °C and incrementally increased to 200 °C, the PO rate, hydrogen consumption rate and hydrogen selectivity consistently tracked one another. The implication of this is that on an increase in temperature, the PO production rate increased faster than the rate of combustion of hydrogen to form water. Because the combustion of hydrogen appears to be a result of dissociation of hydrogen peroxide to form two surface hydroxides that are further reacted to form water [15], it would appear that increasing the temperature does not benefit this peroxide decomposition as much as it makes either propylene or hydrogen peroxide more available for the surface reaction. By 200 °C, the hydrogen consumption rate and PO production rate appeared to be proportional, because a change in reaction temperature from 185 to 200 °C resulted in no change in hydrogen selectivity. Traditional arguments found in the literature would suggest that the increased hydrogen selectivity was a result of increased PO production, allowing more propylene to react with hydrogen peroxide before it could decompose [6,15]. At temperatures above 185 °C, PO desorption would no longer be considered to hamper the reaction, and the system would reach its true hydrogen selectivity in the absence of product inhibition. However, because the PO partial pressure was found to have little effect on the PO rate at any temperature, this explanation is inconsistent with the kinetic results presented in this work.

The robustness of the power rate law is shown in Fig. 9 in which kinetic information was collected for a number of points outside of the range of concentrations used in the design of experiments. Although the power rate law appeared to capture the trends in the rate, the absolute value of the rate was underpredicted by the power rate law. The extrapolated predictions would be expected to be less accurate than values inside of the concentration space of the kinetic experiments; however, the inaccuracy of the model fit was increased because the absolute error in the power rate law became larger at high PO rates. These conditions were also well above the concentrations examined in the fitting of the two parameters on which the PO rate is most dependent: hydrogen and oxygen orders. It is noteworthy that the model-predicted values fell beneath those measured in the experiments. It is possible—particularly at high concentrations of hydrogen and oxygen—that the activity of the catalysts was actually increased as a result of the oxidation of carbonacious surface species. Catalysts of this type have been shown previously to be reactivated using thermal treatments in mixtures of hydrogen and oxygen [9].

The parameters obtained from the model provide valuable constraints on mechanisms that are consistent with experimental data. It is not particularly remarkable that all three reactants have fractional orders; however, it is noteworthy that these three fractional orders do not appear to be functionally related. Numerous identical fractional orders, mixtures of fractional orders, and half orders or functional relationships between all of the orders (e.g., the hydrogen order is always twice the oxygen order and the same as the propylene order) are more easily explained in the confines of Langmuir–Hinschelwood kinetics, in which rate expressions take the form of $K[A]/(1 + K[A])$, where K is an equilibrium adsorption constant and [A] is a gas-phase concentration. Kinetic expressions of this form can be approximated as $(K[A])^{\alpha}$, resulting in an apparent fraction reaction order. We note, however, that each such fractional order term requires a separate $[1 + K_i(A_i)]$ term in the denominator, and each term in such a product denominator implies a separate, noncompetitive site in the Langmuir–Hinschelwood formalism. Thus, the three apparently independent reaction or-

$$O_2 + S_1 \leftrightarrow O_2\text{–}S_1 \quad (1)$$

$$H_2 + O_2\text{–}S_1 + S_1 \leftrightarrow HOO\text{–}S_1 + H\text{–}S_1 \quad (2)$$

$$O_2 + 2H\text{–}S_1 \leftrightarrow HOO\text{–}S_1 + H\text{–}S_1 \quad (3)$$

$$H_2 + HOO\text{–}S_1 + S_1 \leftrightarrow HOOH\text{–}S_1 + H\text{–}S_1 \quad (4)$$

Fig. 10. A series of four elementary steps determined using DFT calculations from references 15 and 19 to describe the formation of hydrogen peroxide over a gold site (S_1).

$$C_3H_6 + S_2 \leftrightarrow C_3H_6\text{–}S_2 \quad (5)$$

$$C_3H_6\text{–}S_2 + HOOH\text{–}S_1 \rightarrow H_2O\text{–}S_1 + PO\text{–}S_2 \quad (6)$$

$$PO\text{–}S_2 \leftrightarrow PO + S_2 \quad (7)$$

$$H_2O\text{–}S_1 \leftrightarrow H_2O + S_1 \quad (8)$$

Fig. 11. A series of four elementary steps developed in conjunction with the mechanism presented in Fig. 6 and implied by the fractional reaction orders obtained in this work. Step 6 is considered to be the RDS.

ders extracted from these data ensure that, at the very least, two active sites must be involved in rate-determining step (RDS).

The construction of a viable mechanism for the epoxidation of propylene over Au/TS-1 catalysts must take into account the apparent bi-functionality of the catalyst. The experimental [16–18] and computational [15,19] evidence of in situ oxidant formation over a gold species, followed by epoxidation by a titanium species [5,20,21], is a reasonable starting point for a two-site mechanism capable of fitting these experimental data. The compelling source of information concerning the formation of oxidants using gold as a catalyst comes in the form of DFT calculations [15,19]. Fig. 10 outlines a series of mechanistic steps for the production of hydrogen peroxide as indicated by DFT calculations presented previously in the literature, where S_1 indicates an active gold site. The reaction is shown to proceed somewhat differently than would generally be written for surface reactions. Hydrogen appears to be incapable of adsorbing on a bare gold surface; instead, its adsorption is promoted by the presence of molecular oxygen on the surface. This reaction with oxygen produces a hydroperoxy intermediate and an adsorbed hydrogen atom. Rather than simple addition of the atomic surface hydrogen to the hydroperoxy intermediate to complete the formation of hydrogen peroxide, a second hydrogen molecule reacts from the gas phase directly with the hydroperoxy intermediate to form hydrogen peroxide and more adsorbed hydrogen. With the desorption, reaction, or decomposition of hydrogen peroxide, the surface is left with adsorbed hydrogen atoms, which can then react with gas-phase molecular oxygen to again form a hydroperoxy intermediate. At no point is there an explicit hydrogen dissociation step, but a linear combination of Eqs. (1)–(3) does produce an effective dissociation step. The necessity for an oxygen-covered surface to begin the catalytic cycle is also supported by the saturation in the PO rate with oxygen partial pressure, as shown in this work and in that of Haruta et al. [1].

All of the remaining mechanistic steps necessary to produce PO have been placed at the titanium reaction center, denoted by S_2, as shown in Fig. 11. The primary purpose of this site is to adsorb propylene so that it can be further reacted to form PO. This begins with a standard adsorption step. The reaction of propylene to form PO must be the RDS and must include both active sites; otherwise, the observed fractional reaction orders cannot be reproduced. This results in a surface reaction involving both adsorbed propylene on a titanium center and hydrogen peroxide on an active gold site. For the sake of this model, this surface reaction is said to produce PO on a titanium center and water on an active gold site; however, the details of this aspect of the site chemistry are not clear, because these species appear after the RDS and thus do not appear in the rate expression derived from these elementary steps. The placement of water on a gold site seems to be a reasonable assumption, because gold nanoparticles in the absence of titanium have been shown to catalyze the combustion of hydrogen to form water [16,18]. The mechanism completes with desorption of PO and water from the titanium and gold sites respectively.

Considering step 6 of Fig. 11 to be the RDS, the rate expression for PO production takes the form shown in Eq. (1), where k_6 indicates the forward rate constant, $z[\text{HOOH–S}_1]/L_1$ indicates the probability of finding [HOOH–S_1] surface intermediates adjacent to [C_3H_6–S_2] species, L_1 indicates the total number of active gold sites, and [HOOH–S_1] and [C_3H_6–S_2] denote surface concentrations of hydrogen peroxide on S_1 and propylene on S_2, respectively:

$$\text{Rate}_{PO} = \frac{k_6 z}{L_1}[C_3H_6\text{–}S_2][HOOH\text{–}S_1]. \quad (1)$$

Assuming that all other steps from the combined mechanism of Figs. 10 and 11 are at quasi equilibrium and that the most abundant reactive intermediate (MARI) for the titanium sites is propylene and for the gold sites is the hydroperoxy intermediate, the rate law presented as Eq. (2) results:

$$\text{Rate}_{PO} = \frac{k_6 z}{L_1}\left[\frac{L_1 K_5[C_3H_6]}{1 + K_5[C_3H_6]}\right]\left[\frac{L_2 K_3^{1/2} K_4 [H_2]^{1/2}}{K_1^{1/2} K_2^{1/2}}\right] \times \left[\frac{K_1^{1/2} K_2^{1/2} K_3^{1/2} [H_2]^{1/2}[O_2]}{1 + K_1^{1/2} K_2^{1/2} K_3^{1/2} [H_2]^{1/2}[O_2]}\right]. \quad (2)$$

This expression has already been factored into three portions such that two of the portions are of the form $K[A]/(1 + K[A])$, which can be approximated by $(K[A])^{\alpha}$. Using this simplification, Eq. (3) is obtained:

$$\text{Rate}_{PO} = k_6 z L_2 \left[K_5[C_3H_6]\right]^n \left[\frac{K_3^{1/2} K_4 [H_2]^{1/2}}{K_1^{1/2} K_2^{1/2}}\right] \times \left[K_1^{1/2} K_2^{1/2} K_3^{1/2} [H_2]^{1/2}[O_2]\right]^{2m}. \quad (3)$$

The power rate law expression extracted from the hybridized factorial design of kinetic experiments provides the reaction orders for each of the reactants. As shown in Table 2, the propylene order was 0.18 ± 0.04, the hydrogen order was 0.60 ± 0.03. and the oxygen order was 0.31 ± 0.04. Substituting $n = 0.18$ and $2m = 0.28$, the experimental reaction orders were nearly equivalent, given the error in the experimental measurements, to those of the proposed reaction mechanism.

It should not be ignored that the ratio of the hydrogen and oxygen order was essentially 2, which would generally imply

a much simpler relationship between the hydrogen order and oxygen order obtained from a series of elementary steps (e.g., nondissociative hydrogen adsorption and dissociative oxygen absorption). The complication is that no sequence of elementary steps yet proposed or known to occur over gold catalysts of this type is capable of reproducing a hydrogen order twice that of oxygen. Presumably, because neither the oxygen nor the hydrogen order is 0.5 or 1, the rate expression would have to take the form $K[H_2][O_2]^{1/2}/(1 + K[H_2][O_2]^{1/2})$, which would predict rate saturation at high hydrogen and high oxygen coverage. But although PO rate saturation was observed at high oxygen partial pressures, there was no evidence of a similar effect by hydrogen at feed concentrations up to 40 mol%. The two-step addition of hydrogen, as shown by DFT calculations, is the only way that we have found to produce hydrogen orders higher than that of oxygen and in excess of 0.5, which is required by the power rate law obtained in this work and consistent with the generation and subsequent reaction of hydroperoxy and hydrogen peroxide-like species.

The two-site mechanism presented here is the simplest means of reproducing the kinetic data obtained from this system. Hydrogen oxidation was extensively studied by Barton et al. over Au/SiO_2, Au/TS-1, and Au/S-1 catalysts [15]. Although the observed hydrogen and oxygen reactant orders were similar to those obtained in this work (0.69–0.82 and 0.08–0.19, respectively), the lack of a functional relationship between the orders necessitated a mechanism with two sites participating in the RDS. The fractional propylene order for the gas-phase epoxidation requires that propylene participate in the RDS, which would force the overall mechanism to consist of three active sites working in concert to reproduce the experimentally determined orders of this work. Any number of three site mechanisms would be capable of reproducing this data, because introduction of the third site (most likely a hydrogen adsorption site) would provide direct control over all three of the reactant orders, but little mechanistic insight.

The mechanism leading to Eq. (3) differs from many proposed in the literature (in the absence of supporting kinetic data) in that the RDS truly involves two different active sites. It has been proposed previously that hydrogen peroxide or a hydropropoxy intermediate was formed over an active gold species, followed by spillover of that oxidant to a titanium site, followed by epoxidation of propylene at the epoxidation site [5]. This view is rooted in the observation that hydrogen peroxide will epoxidize propylene in liquid-phase reactions using TS-1 as the catalyst [20], and the observation that mixtures of hydrogen and oxygen can produce hydrogen peroxide over gold catalysts [16–18]. However, this reaction mechanism is not consistent with the experimentally determined orders of reaction. Migration of hydroperoxy species or hydrogen peroxide to a titanium center followed by epoxidation would (1) force the hydrogen and oxygen orders to unobserved values (either they would be the same or hydrogen order would be half that of oxygen) and propylene to be either zero or first order, (2) cause propylene to be fractional order and hydrogen and oxygen to be either both first order, or (3) cause propylene to be fractional order and oxygen to be first order and hydrogen half order, depending on the mechanism for hydrogen addition to adsorbed oxygen. In any case, an RDS involving a single reaction site is ultimately insufficient to reproduce the experimental reaction orders, particularly the observation that the hydrogen order is higher than the oxygen order.

It has also been noted in the literature that propylene adsorbs on Au/TiO_2 surfaces to produce surface species nearly identical to that of adsorbed PO, resulting in the assertion that the presence of gold activates propylene for epoxidation [22,23]. Similarly, it also has been shown, using $Au/TiO_2(110)$ model catalysts and temperature-programmed desorption experiments, that propylene adsorbs initially at interfacial sites [24]. DFT calculations have also shown that in the absence of hydrogen peroxide, propylene interacts very little with the titanium center in TS-1 [21]. Although our proposed mechanism places propylene at the titanium center, there is nothing in the mechanism that would prevent activation of propylene at a gold site. In fact, it would be premature to use any of this information to specifically designate S_2 as any more than an active site containing titanium, because no specifics on the active site are explicitly provided by kinetic analysis. What this mechanism does suggest is that propylene activation is not rate-determining, nor is propylene the dominant surface species on gold sites. That being said, it is possible to consider S_2 as an interfacial site that is somehow bridging the active gold ensemble and titanium site. This would allow for activation in the presence of gold while a second, distinct population of gold generates the oxidant. If, for example, the RDS reported in Fig. 11 were reversed such that hydrogen peroxide or hydroperoxy species were produced on gold sites and spilled over to a titanium center, which then reacted with propylene adsorbed on gold sites, then either the oxygen and hydrogen orders would be identical or the hydrogen order would be half that of oxygen while propylene could have any order between zero and one. The positioning of the oxidant on the gold sites is necessary to reproduce the experimentally observed orders in this study, and thus positioning of the propylene near some kind of titanium containing site is also required.

Perhaps the most comprehensive kinetic study on catalysts of the Au/TS-1 family was completed through the examination of complete hydrogen combustion to form water [15]. To accurately account for the reaction orders of hydrogen and oxygen, a two-site mechanism had to be adopted. Although the apparent activation energies observed for water synthesis (37–41 kJ/mol) were close to the 35 kJ/mol observed in this study for catalysts 0.04Au/TS-1(143) and 0.06Au/TS-1(36), the addition of a rate dependence on propylene concentration would require an additional active site. As discussed previously, three sites would allow independent control of all reactant orders, but would not provide much constraint on the elementary steps that result in propylene epoxidation. Furthermore, a third site adds complexity that may not be justified. The similarity in apparent activation energies for PO formation versus hydrogen combustion would suggest that although the rate-limiting formation of hydrogen peroxide described previously [15] is not the same RDS as in our system, the mechanisms appear to be energetically similar.

5. Conclusion

A design of experiments was used to complete the first kinetic analysis of propylene epoxidation over Au/TS-1 catalysts in the absence of significant deactivation. A power rate law for the production of PO was extracted from 33 experiments of the factorial design for 3 catalysts prepared with differing metal loadings and different TS-1 supports. These orders were used to show that a minimum of two active sites must work in conjunction to produce the experimentally observed orders. A two-site mechanism was presented that accounts for these orders by producing hydrogen peroxide over gold sites and reacting it with propylene adsorbed at a titanium site. The PO rate was found to be most dependent on hydrogen with an order of 0.60, compared with 0.31 for oxygen and 0.18 for propylene. The experimental reaction orders were matched with mechanistic insight provided by DFT calculations and by assuming that the most abundant reactive intermediate on the active gold sites was a hydroperoxy species and that the most abundant species on the titanium-containing site was adsorbed propylene. Quantification of hydrogen consumption showed that hydrogen combustion was strongly related to hydrogen concentration in the reactant mixture and that catalyst activation in a 10/10/10/70 vol% $O_2/H_2/C_3H_6/N_2$ reactant mixture at 200 °C produced the highest hydrogen selectivity. Alteration of this atmosphere to a 5/12/12/71 vol% $O_2/H_2/C_3H_6/N_2$ irreversibly decreased the hydrogen efficiency. Hydrogen consumption, hydrogen selectivity, and PO rate were all found to increase incrementally with increases in temperature up to 200 °C, implying that in the activation, energy for PO production was less than that for water production. Ultimately, despite changes in reaction conditions, the hydrogen selectivity was generally between 7 and 15%.

Acknowledgments

Support for this research was provided by the United States Department of Energy, Office of Basic Energy Sciences through grant DE-FG02-01ER-15107.

Appendix A

To allow alternative analyses of the data, the average rate values and the actual compositions for the experiments depicted in Fig. 1 are presented for 0.04Au/TS-1(143) in Table A1, for 0.06Au/TS-1(36) in Table A2, and for 0.02Au/TS-1(36) in Table A3.

Table A1
Compositions and rate data for 0.04Au/TS-1(143). The run numbers and temperatures correspond to those in Fig. 1

Exp. #	Reactant volume (%)			PO rate ($g_{PO}/(h\,kg_{cat})$)
	O_2	H_2	C_3H_6	
1	3.73	10.75	10.15	18.60
2	3.86	10.98	10.25	9.32
3	3.77	10.85	10.21	12.92
4	3.58	10.47	9.98	24.45
5	3.43	10.14	9.66	28.49
6	3.73	10.71	10.15	17.06
7	1.35	11.25	10.47	12.59
8	2.52	10.98	10.24	14.53
9	4.98	10.65	10.06	17.83
10	5.95	10.60	10.09	18.48
11	3.55	10.13	9.70	14.95
12	3.97	6.96	10.11	12.20
13	3.41	13.83	9.58	17.90
14	3.53	10.09	7.12	14.06
15	3.53	10.08	12.01	15.76
16	3.57	10.14	9.61	14.90
17	2.33	14.28	11.95	11.79
18	2.11	21.67	7.23	12.88
19	2.50	6.71	16.54	7.98
20	2.52	6.78	7.47	7.14
21	1.93	17.29	9.06	23.83
22	2.20	10.00	13.92	19.03
23	2.06	13.87	6.87	19.35
24	2.65	3.68	12.60	8.91
25	4.83	6.42	16.07	9.54
26	4.56	13.60	11.84	14.18
27	4.86	6.55	7.18	8.56
28	4.35	20.89	6.99	15.94
29	4.16	15.68	8.20	32.83
31	4.30	13.13	6.68	25.93
32	4.69	6.30	11.86	16.64
30	4.44	9.67	13.44	20.75
33	3.50	9.91	9.53	13.07

Table A2
Compositions and rate data for 0.06Au/TS-1(36). The run numbers and temperatures correspond to those in Fig. 1

Exp. #	Reactant volume (%)			PO rate ($g_{PO}/(h\,kg_{cat})$)
	O_2	H_2	C_3H_6	
1	4.41	9.63	10.44	24.99
2	4.42	10.25	10.53	12.38
3	4.69	10.03	10.47	17.43
4	3.91	9.54	10.50	31.36
5	3.62	9.22	10.46	37.81
6	4.37	9.83	10.49	22.81
7	1.46	9.81	9.61	16.68
8	2.95	9.56	9.82	20.60
9	5.15	8.54	9.63	22.78
10	6.13	8.28	9.69	23.99
11	4.12	8.91	9.61	21.51
12	3.95	5.45	9.82	15.04
13	4.85	13.10	9.58	25.13
14	4.34	9.11	6.57	18.86
15	4.28	9.02	12.66	21.17
16	4.11	9.08	9.73	20.47
17	4.36	9.15	9.80	20.47
18	3.67	13.89	12.87	16.92
19	3.30	22.88	6.44	17.85
20	3.01	5.85	19.73	10.92
21	2.88	6.00	6.66	8.99
22	2.74	17.67	9.72	34.37
23	3.07	9.28	16.23	26.99
24	2.65	5.67	13.03	19.06
25	3.25	13.43	6.58	28.33
26	5.26	5.58	19.59	12.17
27	6.22	13.06	12.95	19.66
28	5.14	5.53	6.84	10.29
29	7.43	21.83	6.65	21.22
30	5.06	8.40	15.97	26.19
31	5.51	12.46	6.45	27.28
32	4.86	5.06	13.00	18.46
33	4.24	8.90	9.65	17.16

Table A3
Compositions and rate data for 0.02Au/TS-1(36). The run numbers and temperatures correspond to those in Fig. 1

Exp. #	Reactant volume (%)			PO rate ($g_{PO}/(h\,kg_{cat})$)
	O_2	H_2	C_3H_6	
1	4.53	10.22	9.76	2.95
2	4.75	10.28	9.69	0.92
3	4.62	10.25	9.67	1.58
4	4.53	10.20	9.67	4.18
5	4.60	10.21	9.68	5.57
6	4.70	10.37	9.74	2.48
7	2.35	10.84	9.94	2.15
8	3.67	10.73	9.95	2.42
9	5.85	10.60	9.98	2.59
10	7.00	10.52	9.97	2.72
11	4.66	10.64	9.92	2.45
12	4.24	6.80	10.06	1.87
13	5.36	15.05	10.00	3.22
14	4.67	10.78	6.86	2.45
15	4.71	10.71	13.22	2.70
16	5.02	11.10	10.46	2.62
17	4.35	15.43	13.50	1.80
18	5.45	23.98	7.01	2.38
19	3.22	6.87	19.63	1.21
20	3.19	7.02	6.98	0.95
21	5.03	19.45	10.24	6.06
22	3.76	10.91	16.58	4.19
23	3.14	6.94	13.52	2.93
24	4.26	15.32	7.02	5.04
25	5.43	6.92	19.57	1.33
26	6.77	15.12	13.25	2.24
27	5.36	6.78	6.88	1.08
28	7.91	23.55	6.79	2.65
29	7.32	19.57	10.31	7.18
30	5.89	10.90	16.37	5.41
31	6.63	15.08	6.91	5.85
32	5.34	6.76	13.27	3.47
33	4.80	10.87	10.06	2.67

References

[1] T. Hayashi, K. Tanaka, M. Haruta, J. Catal. 178 (1998) 566.
[2] E.E. Stangland, K.B. Stavens, R.P. Andres, W.N. Delgass, Stud. Surf. Sci. Catal. 130 (2000) 827.
[3] E.E. Stangland, K.B. Stavens, R.P. Andres, W.N. Delgass, J. Catal. 191 (2000) 332.
[4] M. Haruta, M. Date, Appl. Catal. A 222 (2001) 427.
[5] T.A. Nijhuis, B.J. Huizinga, M. Makkee, J.A. Moulijn, Ind. Eng. Chem. Res. 38 (1999) 884.
[6] C. Qi, T. Akita, M. Okumura, M. Haruta, Appl. Catal. A 218 (2001) 81.
[7] G. Mul, A. Swijnenburg, B. van der Linden, M. Makkee, J.A. Moulijn, J. Catal. 201 (2001) 128.
[8] E.E. Stangland, B. Taylor, R.P. Andres, W.N. Delgass, J. Phys. Chem. B 109 (2005) 2321.
[9] A.K. Sinha, S. Seelan, S. Tsubota, M. Haruta, Angew. Chem. 43 (2004) 1546.
[10] B. Taylor, J. Lauterbach, W.N. Delgass, Appl. Catal. A Gen. 291 (2005) 188.
[11] R.B. Khomane, D.B. Kulkarni, A. Paraskar, S.R. Sainkar, Mater. Chem. Phys. 76 (2002) 227.
[12] S. Tsubota, D.A.H. Cunningham, Y. Bando, M. Haruta, Stud. Surf. Sci. Catal. 91 (1995) 227.
[13] M. Date, M. Haruta, J. Catal. 201 (2001) 221.
[14] T.A. Nijhuis, B.M. Weckhuysen, Chem. Commun. (2005) 6002.
[15] D.G. Barton, S.G. Podkolzin, J. Phys. Chem. B 109 (2005) 2262.
[16] M. Okumura, Y. Kitagawa, K. Yamaguchi, T. Akita, S. Tsubota, M. Haruta, Chem. Lett. 32 (2003) 822.
[17] C. Sivandinarayana, T.V. Choudhardy, L.L. Daemen, J. Eckert, D.W. Goodman, J. Am. Chem. Soc. Commun. 126 (2004) 38.
[18] P. Landon, P.J. Collier, A.J. Papworth, C.J. Kiely, G.J. Hutchings, Chem. Commun. 18 (2002) 2058.
[19] D.H. Wells, W.N. Delgass, K.T. Thomson, J. Catal. 225 (2004) 69.
[20] M.G. Clerici, G. Bellussi, U. Romano, J. Catal. 129 (1991) 159.
[21] D.H. Wells, W.N. Delgass, K.T. Thomson, J. Am. Chem. Soc. 126 (2004) 2956.
[22] T.A. Nijhuis, T. Visser, B.M. Weckhuysen, Angew. Chem. Int. Ed. 44 (2005) 1115.
[23] T.A. Nijhuis, T.Q. Gardner, B.M. Weckhuysen, J. Catal. 236 (2005) 153.
[24] H.M. Ajo, V.A. Bondzie, C.T. Campbell, Catal. Lett. 78 (2002) 359.